3-D Time-Accurate CFD Simulations of a Multi-Megawatt Slender Bladed HAWT under Yawed Inflow Conditions

M. Sayed, Th. Lutz and E. Krämer

Institute of Aerodynamics and Gas Dynamics (IAG), University of Stuttgart, Pfaffenwaldring 21, D-70569 Stuttgart

E-mail: sayed@iag.uni-stuttgart.de

Abstract. In the present study numerical investigations of a generic Multi-Megawatt slender bladed Horizontal-Axis Wind Turbine (HAWT) under yawed inflow conditions were conducted. A three-dimensional URANS flow solver based on structured overlapping meshes was used. The simulations were conducted at wind speeds of 7 m/sec, 11 m/sec and 15 m/sec for different yaw angles ranging from $+60^\circ$ to -60°. It was concluded that, for below rated wind speeds, under small yaw angles (below $\pm 15^\circ$) the magnitudes of the blade forces are slightly increased, while under high yaw angles (above $\pm 15^\circ$) there is a significant decrease. Moreover, the load fluctuations, for the different yaw angles, have the same frequency but different amplitude and oscillation shape. It was concluded that at the above rated wind speed of 15 m/sec, the blade aerodynamic loads are significantly affected by the yaw inflow conditions and the magnitude values of the loads are decreased with increasing yaw angle. It can be concluded that the angle of attack and the tower interference are the utmost variables affecting the yawed turbines.

1. Introduction

As the wind direction is always random and continuously changing, HAWTs are basically exposed to yawed flow conditions most of their operating time. Under these conditions, highly unsteady flow conditions over the wind turbine blades is introduced due to a parallel velocity component to the rotor disk. This unsteadiness results from strong radial flow along the span-wise as well as dynamic stall on the blade and also leading edge separation bubbles [1]. As a result, the rotor performance is strongly affected due to the blade load fluctuations which will also affect the operational life of the wind turbine. Consequently, it is important to understand the flow unsteadiness under yawed turbine operation conditions for better further development in the future.

Different aerodynamic methods are used to solve the flow field around the wind turbine. These methods vary in their degree of complexity and accuracy ranging from Blade Element Momentum theory (BEM) and lifting line theory [2] to the solution of Navier-Stokes equations using Computational Fluid Dynamics (CFD). Simplified methods such as the lifting line theory were used in [1] and [2] to investigate the aerodynamic loads of the wind turbine under yaw conditions. Simulations for yaw angles of 10°, 30° and 60° were performed at a wind speed of 10 m/sec. The results showed that the method cannot capture the dynamic stall and stall delay

and therefore, a dynamic stall model should be included to improve the accuracy of the results. CFD models of wind turbines have been widely used, as in [3], [4], [5], [6], [7], [8] and [9], to capture the flow phenomena that cannot be resolved using simplified numerical methods. CFD simulations of a compressible Euler flow using unstructured meshes were performed in [6]. This aerodynamic model was used because of an inviscid flow assumption at this wind speed. Only one flow case was investigated at a yaw angle of 30° and a low wind speed of 7 m/sec.

Simulations of yawed wind turbines based on the solution the Navier-Stokes equations were examined in literature. A structured mesh flow solver combined with a BEM model were used to investigate the wind turbine at a yaw angle of 45° for a low wind speed of 7 m/sec [7]. It was concluded that the classical inflow model used in the BEM should be improved to accurately capture the downwash flow of the rotor. Moreover, a hybrid Navier-Stokes/Vortex-wake method coupled to a turbulence model of BaldwinLomax was used to investigate the blade loadings at different flow cases [8]. But there were no detailed studies on the time-accurate blade loadings.

In the present paper, 3-D time-accurate CFD simulations were conducted on a multi-megawatt HAWT rotor under yawed inflow conditions. The simulations were performed at wind speeds of 7 m/sec, 11 m/sec and 15 m/sec for different yaw angles ranging from +60° to −60°. The blade loads are used to present and discuss the time-accurate results and detailed flow features over the blades are also observed.

2. Methodology

2.1. Wind Turbine configuration

The wind turbine examined in the present study is the generic reference turbine of the ongoing European InnWind project [10] designed by DTU. It is a large HAWT with 178.3 m rotor diameter, a hub height of 119 m and FFA-W3 airfoil series. The rotor is installed at 5° tilt angle and a cone angle of −2.5°. The solid modelling of the complete wind turbine is presented in Figure 1, in which the used coordinate system, wind direction and yaw and azimuthal directions are defined. For the present simulations, all the wind turbine components are assumed to be rigid. A cylindrical tower is considered with 8.3 m outer diameter at the ground and 5.5 m outer diameter at the top. The wind turbine rotor rotates clockwise as viewed from the inlet boundary. Pre-bended blades are used with about 3.73%R at the blade tip. The blade at the root region is equipped with wedge shaped Gurney flaps to increase the aerodynamic performance [10].

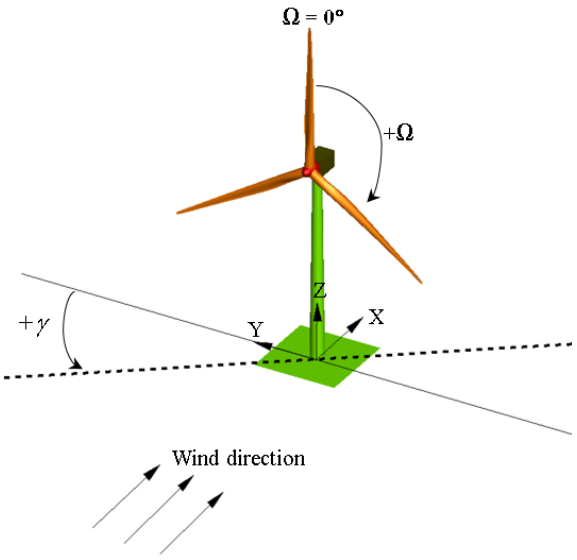

Figure 1: Wind turbine configuration and definitions of global coordinate system, wind direction, positive yaw and positive azimuthal directions

2.2. Process Chain for Wind Turbine Simulations

The simulations performed here have been achieved with FLOWer [11] which is a block structured flow solver. It is provided by the German Aerospace Center DLR with specific extensions implemented at the IAG. In order to achieve the proposed simulations of the wind turbine, a process starting from generating the geometries of the used model to the final discretized model must be performed. In the recent years, a process chain of the wind turbine simulations was developed at the IAG. This process chain includes a user friendly script for blade grid generation in purpose of minimizing the effort in the blade meshing process. Hence the blade mesh is the most important key feature in the turbine simulations, one must carefully set the different parameters in the script to insure the quality of the generated mesh. Several CFD simulations of different offshore and onshore wind turbines have been conducted using that process chain at IAG [12], [13] and [14]. These CFD simulations proof the quality of the used process chain at the IAG.

2.3. Computational Domain

In this paper, a structured overset mesh technique is used to generate the computational domains. This overset feature allows more mesh control over all the wind turbine parts, as every component was meshed separately and finally the domains are placed together and overlapped using CHIMERA overlapping mesh technique. The computational domain of the whole turbine consist of three blades, hub, nacelle and tower. The meshes were generated using Gridgen®. The blade mesh was generated and refined by the developed script at IAG. For each sub-domain, an independent grid was created with adopted refinement. Finally a background mesh was created to extend the computational domain to the far field [14]. The grid statistics of the different domains used in the simulations are as shown in Table 1 and Figure 2.

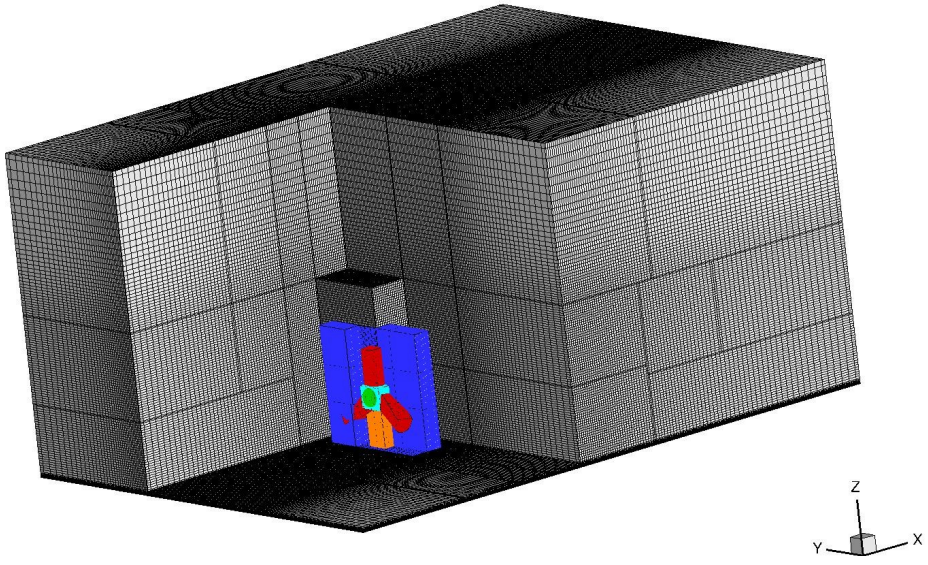

Figure 2: The assembled domains, Red are blades domains, Orange is the tower domain, Green represents the hub domain, Cyan shows the nacelle domain, Blue is the fine background domain and Black is the extended background domain

Two different background meshes were used. The first one is the coarse background mesh with cell size of 5 m in all directions around the turbine and cell size of 20m at the far field boundaries. This domain has a cubic shape (as show in Figure 2) with dimensions of 6R in the upstream direction, 9R in the downstream direction, 8R in the far field direction and 6R in each of the horizontal direction. These values are used based on studies done by [14]. At the ground, the mesh was refined to account for the boundary layer at the ground. The second

Table 1: Grid statistics

Domain	Number of cells [*million*]
Blade	6.5
Tower	1.15
Hub	2.2
Nacelle	1.75
Fine Background	0.9
Extended Background	3.1
Blade-Hub Connector	0.8
Total Number of Cells	31

one is the fine background mesh with 2m cell size in all directions. This domain has a cubic shape with dimensions of 1R×3R×3R in the $x-$, $y-$, $z-$direction respectively. It is used only to avoid having the whole background mesh as a fine mesh which is too costly and also to get good overlapped regions. Both are non-rotating meshes. The tower mesh has an outer cubic shape with 0.5R in x- and y-direction. The grid size at the outer boundary is 0.8m and refined close to the surface of the tower to fulfill the $y^+ \leq 1$ condition at the first grid cell. A no-slip boundary condition is applied to the tower surface. The nacelle mesh was also generated taking into account the $y^+ \leq 1$ condition at the nacelle wall and also the no-slip boundary condition is applied. The cell size at the nacelle surface is 0.3 m and it is the last non-rotating grid. The hub mesh was generated and it is the first rotating mesh in this setup. It was connected to a rotating blade-hub-connector mesh and the non-rotating nacelle mesh. The hub rotation is around the rotor axis as defined before at 5° tilt angle.

Finally the blade mesh was generated (blade sectional mesh is shown in Figure 3) using the proven script at the IAG [13] and [15]. 300 cells were used in chord-wise direction and 100 cells in (span-wise) radial direction. 35 cells were introduced to resolve the boundary layer with $y^+ \approx 1$ for the first boundary layer cells. The time-step was equivalent to 3° azimuthal-step. These values were chosen based on studies performed at IAG [14]. The turbulence model used in the simulations is the Wilcox k-ω turbulence model [16] with fully turbulent flow state. The k-ω model has been successfully used to simulate the flow over airfoils and wind turbines. Moreover, it has been used in many wind-turbine CFD studies such as [1], [3] and [14]. All simulations were performed on the Cray XE6 (HLRS) named HORNET using 448 cores

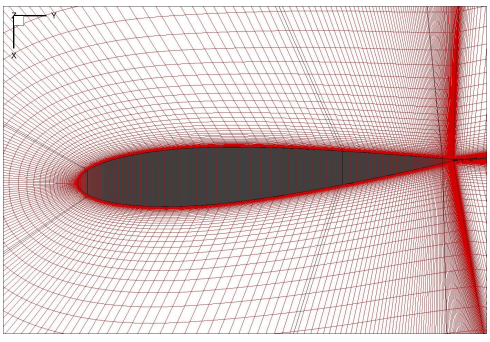

Figure 3: Blade profile meshing at $r = 0.8R$

3. Results

In the present study, the simulations were performed for wind speeds of 7, 11 and 15 m/sec at the yaw angles (γ) of $-60°$, $-45°$, $-30°$, $-15°$, $0°$, $15°$, $30°$, $45°$ and $60°$. As designed, rotor rotational speeds of 6, 8.83564 and 9.6 RPM were used respectively for the used wind speeds. The reason of choosing these wind speeds was to investigate the wind turbine at minimum,

rated and maximum rotational speed. Analyzing yawed inflow conditions can be done either by yawing the wind turbine and keeping the wind direction constant (as in this article) or by keeping the turbine fixed and yawing the wind direction. As the wind turbine is assembled, it was easier to rotate the wind turbine around the $z-$axis by rotating the tower. Because all other components are in the tower coordinate system, all other parts will be rotated as the tower rotates.

For each case, the simulations were performed until periodic unsteady blade aerodynamic loadings were obtained. 25 revolutions were simulated in order to ensure the convergence of the load values, then the results of the last rotor revolution are evaluated. The time-averaged and unsteady time-varying results for the last rotor revolution are presented in form of the blade surface pressure and the normal and tangential force coefficients. Detailed analyses of the flow physics are presented and analyzed to study the dynamic nature of the rotor behavior at yaw misalignment.

3.1. Effects of Yawed Inflow on Wind Turbine Power

As the most important factor in the design of the wind turbine is the power output, the effect of the yawed inflow conditions on the wind turbine power and thrust is studied. The effect of the yawed inflow on the power coefficient C_p and the thrust coefficient C_a is shown in Figure 4. The presented values are a result of time-averaging over the last rotor revolution and then normalized by the results for 0° yaw angle (Baseline). As shown, for small yaw angles between $+15°$ and $-15°$ there is a slight increase in both values of C_p and C_a with respect to the baseline. The reason for that might be that under these small yaw angles there is stall delay which means more attached flow over the blade in the advancing half of the rotor plane. Then for the higher yaw angles, a sudden decrease can be observed of about ≈70% of the C_p and ≈40% of the C_a of the baseline at $\pm 60°$ yaw angles. These values are for the wind speeds of 7 m/sec and 11 m/sec as shown in Table 2. In addition severe reduction is predicted in case of 15 m/sec where negative values are obtained at the $\pm 60°$ yaw angles. As the CFD simulations were performed without controller, i.e constant RPM of 9.6 and constant pitch angle, negative power values were predicted due to negative blade forces in the advancing half of the rotor as a result of geometrical tilt, precone and twist angle and yaw angle.

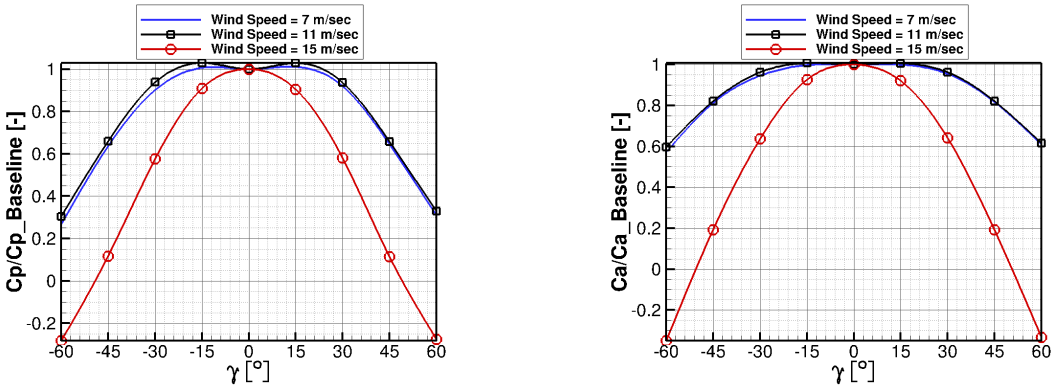

Figure 4: Effect of yawed inflow on the power output at different wind speeds

It was suggested in the literature that the power is reduced by yawed inflow by a cosine-cubed factor (equation 1) and the thrust is reduced by a cosine-squared factor (equation 2) [7] and [17].

$$C_p(\gamma) = C_p(0)cos^3\gamma \tag{1}$$

$$C_a(\gamma) = C_a(0)cos^2\gamma \tag{2}$$

Table 2: Percentage value of the reduction in Power and Thrust

γ [°]	**Wind speeds [m/sec]**					
	7		11		15	
	C_p [%]	C_a [%]	C_p [%]	C_a [%]	C_p [%]	C_a [%]
−60	73	43	69	40	128	135
−45	36	19	34	18	88	81
−30	10	5	6	4	42	36
−15	−1	0	−3	−1	9	7
0	0	0	0	0	0	0
+15	−1	0	−3	−1	9	8
+30	8	5	6	4	42	36
+45	35	18	34	18	89	81
+60	69	39	67	38	128	133

It was also suggested to change the cosines power value in order to find a good matching between the suggested equations and the results. As shown in Figure 5 for the case of 7 m/sec and 11 m/sec, the reduced power and thrust coefficients are not following the reduction factors suggested by [7] and [17]. The reason for that is the slight increase in the C_p and C_a coefficients at small yaw angles. Moreover, in case of 15 m/sec, the suggested factors can be used for yaw angles between ±30° with less than 2% error with cosine power of 3.5 for the power coefficient C_p as shown in Figure 5.

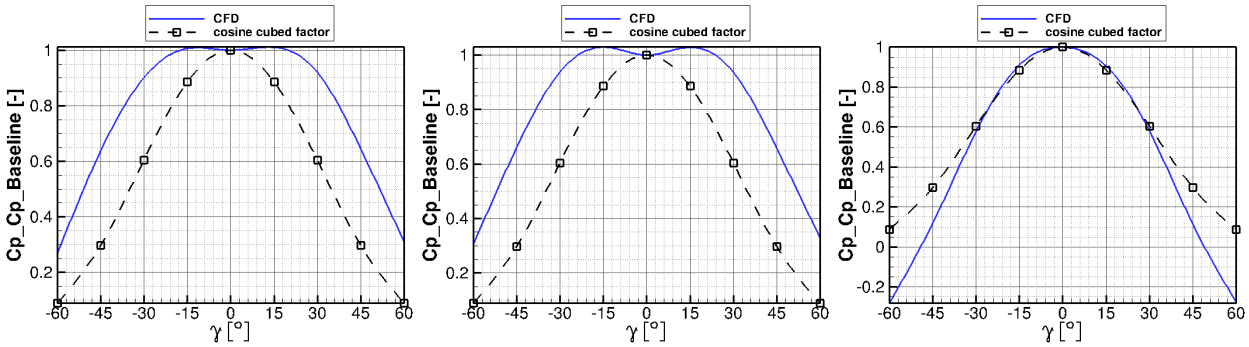

(a) 7 [m/sec] (b) 11 [m/sec] (c) 15 [m/sec]

Figure 5: CFD power coefficients compared to the suggested reduction cosine-cube factor

In addition, the azimuthal variations of the power coefficient C_p are presented for all wind speeds and all yaw angles as shown in Figure 6. In addition to the power reduction, which is also clear in this figure, the power oscillation amplitude is sensitive to the yaw angle as shown in Figure 7. For wind speeds of 7 m/sec and 11 m/sec, the amplitude is minimum at the baseline operating condition of zero yaw. Moreover, larger amplitudes for the positive yaw than for the negative one at the same yaw angle are observed. The oscillation amplitude is smoothly increased till 45° yaw angle and then starts to decrease again. In case of a wind speed of 15 m/sec, the amplitude is 5% which is more than the double for the other wind speeds. The reason for that is the strong tower interference with the rotated blades as there is more reduction in the inflow velocity.

3.2. Effects of Yawed Inflow on Blade loads

3.2.1. Blade loads at a Wind speed of 11 m/sec

First, the simulations were performed for rated wind speed. The loads resulting from the different yawed conditions are also discussed. The azimuthal variation of the normalized thrust and torque is shown in Figure 8. The presented values are normalized by the results for 0° yaw

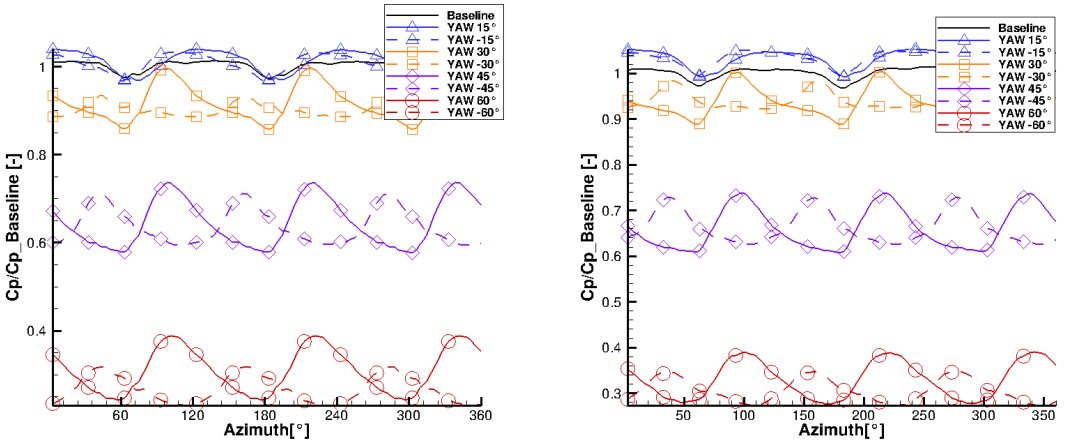

(a) 7 [m/sec]

(b) 11 [m/sec]

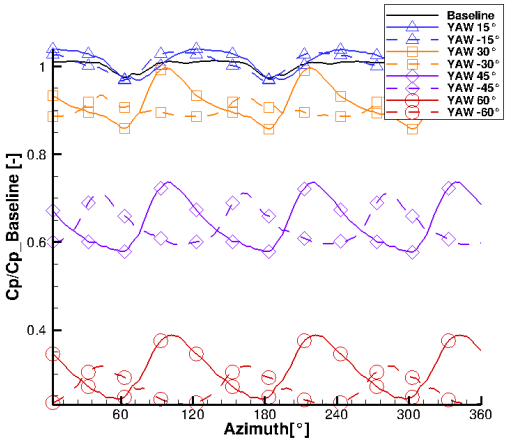

(c) 15 [m/sec]

Figure 6: Effect of yawed inflow on the power output at different wind speeds

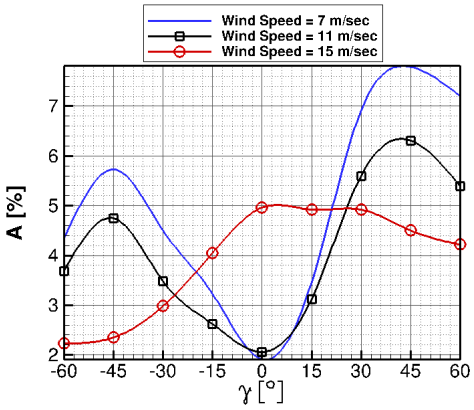

Figure 7: Amplitude variation over the different yaw angles

angle (Baseline). It can be observed that, for small positive yaw angles of less than 30°, there is a slight variation in the thrust about the mean value. There is an increase in the advancing half of the rotor plane (azimuth angle between 90° and 270° for the positive yaw angles), and a slight decrease in the retreating half of the rotor plane (azimuth angle between 270° and 90° for the positive yaw angles).

At 45° there is a dominant increase in the advancing half or the rotor with about 13.5% maximum value at an azimuth angle of 115°. Further increase can be seen at 60° which about 35% higher thrust values were predicted in the advancing half of the rotor at azimuth angle of 120°. For the torque (Figure 8 right), at yaw angles of 15° there is about 20% increase at the

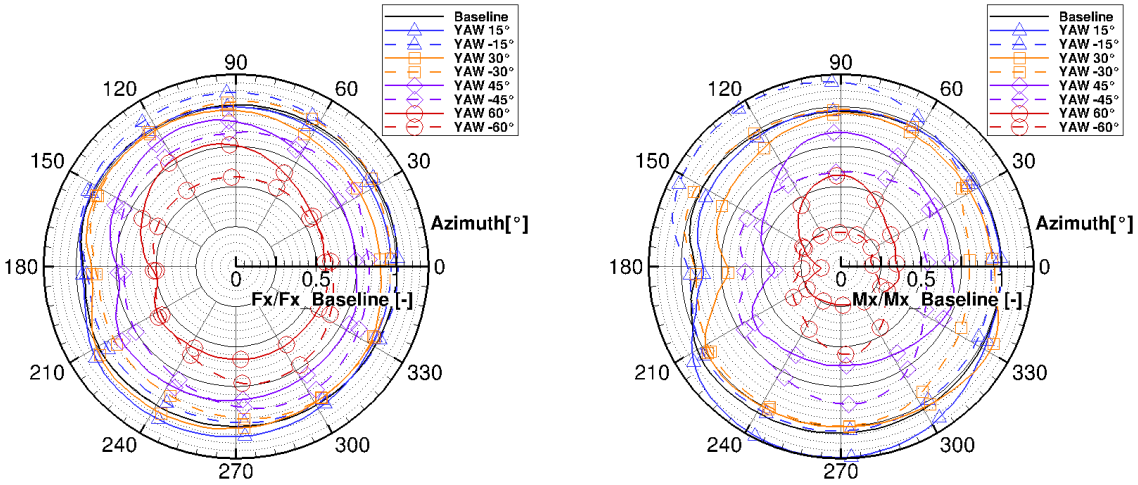

Figure 8: Normalized Thrust (left) and Torque (right) at different yaw angles.

end of the advancing half of the rotor, this is because of the increase in the edge-wise force in the advancing half of the rotor as shown in Figure 9a. At yaw angles of 60° there is about 120% increase in the advancing half of the rotor. The reason behind that is that in the advancing half of the rotor plane the angle of attack increases and hence the blade thrust is increased reaching the maximum at about 120° as shown in Figure 8. In case of negative yawed inflow angles the behavior is inversed.

At an azimuth angle of 180°, the tower interference with blade 1 is seen in Figure 8. The impact increases with increasing yaw angle, the reason for that is the inflow velocity reduction due to the yaw angle. Moreover, it can be concluded that there is more inflow velocity reduction at positive angles than at negative ones. The effect of yaw on the edge-wise force and moment are presented in Figure 9. As shown in Figure 9a, the tower effect is dominant at the baseline. The normalized edge-wise force is reduced by about 15% at the azimuth angle of 180°. Moreover, it is more affected by the tower interference at yaw angle of 45° which is reduced by about 73%. It was expected that in the advancing half of the rotor the edge-wise force will be also increased as in the case of flap-wise forces because of the angle of attack increase. As shown, a slight increase in case of +45° of about 6% is observed. For the edge-wise moment, less tower influence at ±60°, but it is increased by about 60% in the advancing half as shown in Figure 9b.

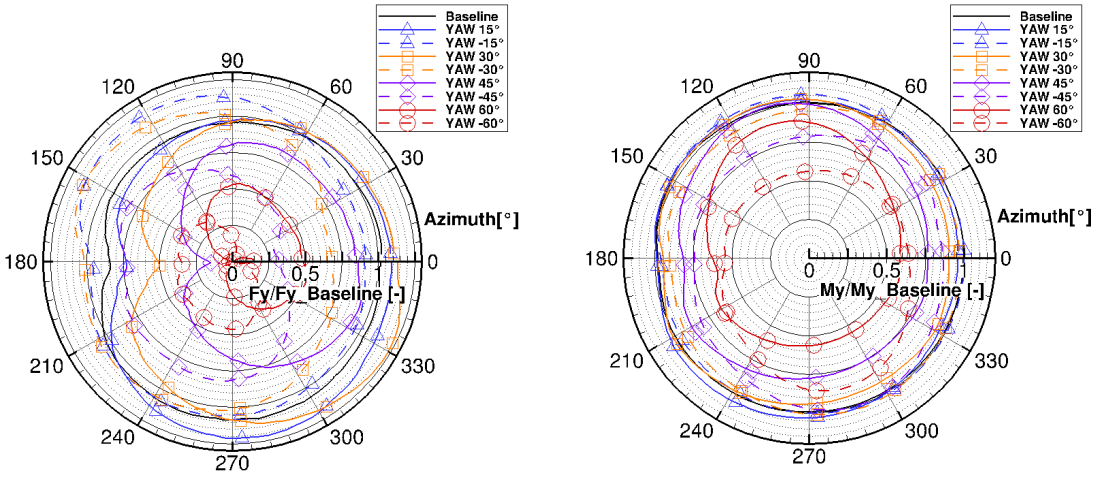

(a) Normalized edge-wise force

(b) Normalized edge-wise moment

Figure 9: Normalized forces and moments of blade 1

These changes in the load values might affect the structural vibration of the blades. Therefore, a Fast Fourier Transform (FFT) was performed. As shown in Figure 10, for the forces, the baseline has the smallest amplitude and as the turbine is yawed the amplitude is increased. It can be concluded that the amplitude is higher for negative yaw compared to the positive one for the same yaw angle except for 60° where both have the same amplitude. In contrast, for the moments, at positive yaw angles the amplitude is slightly higher than at the negative ones. The highest amplitudes are in the advancing half on the rotor, which is expected from the load distribution over one revolution. These high amplitudes will have strong influence on the fatigue and aero-elastic results and should be taken into account.

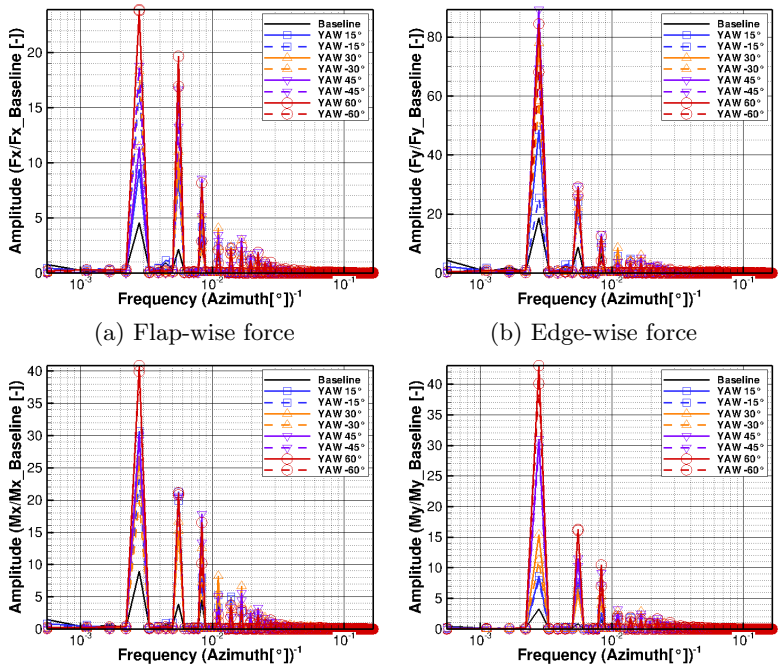

(a) Flap-wise force (b) Edge-wise force

(c) Flap-wise moment (d) Edge-wise moment

Figure 10: FFT of the normalized forces and moments of blade 1

3.2.2. Blade loads at a Wind speed of 7 m/sec

For the wind speed of 7 m/sec, the azimuthal variation of the normalized forces and moments are shown in Figure 12. As described previously, the presented values are normalized with the results of the baseline at the wind speed of 7 m/sec. As shown in Figure 12, it can be concluded that, the yawed inflow at this wind speed has almost the same effect as in the case of 11 m/sec. The reason behind that is that the flow is still attached and the blade is not pitched. Therefore, a slight change occurs for small yaw angles of less than +30°. At yaw angle of +45° there is an increase by about 12.5% of the thrust as shown in (Figure 11a). For +60° an about 33% higher thrust value was predicted in the advancing half of the rotor. For the torque (Figure 11b), at yaw angles of +15° there is about 22% increase in the advancing half of the rotor, this is because of the edge-wise force increase in the advancing half of the rotor as shown in Figure 11c. At yaw angles of +60° there is about 140% increase in the advancing half of the rotor. The reason behind that is that in the advancing half of the rotor there is an increase in the angle of attack and hence the blade thrust is increased reaching the maximum at about 120°. So it can be concluded that for wind speeds less than the rated wind speed, the wind speed has almost no effect on the load distribution and the inflow yawed condition is utmost. The FFT results confirm the same predicted frequencies with very small decrease in the amplitudes compared to the case of 11 m/sec wind speed.

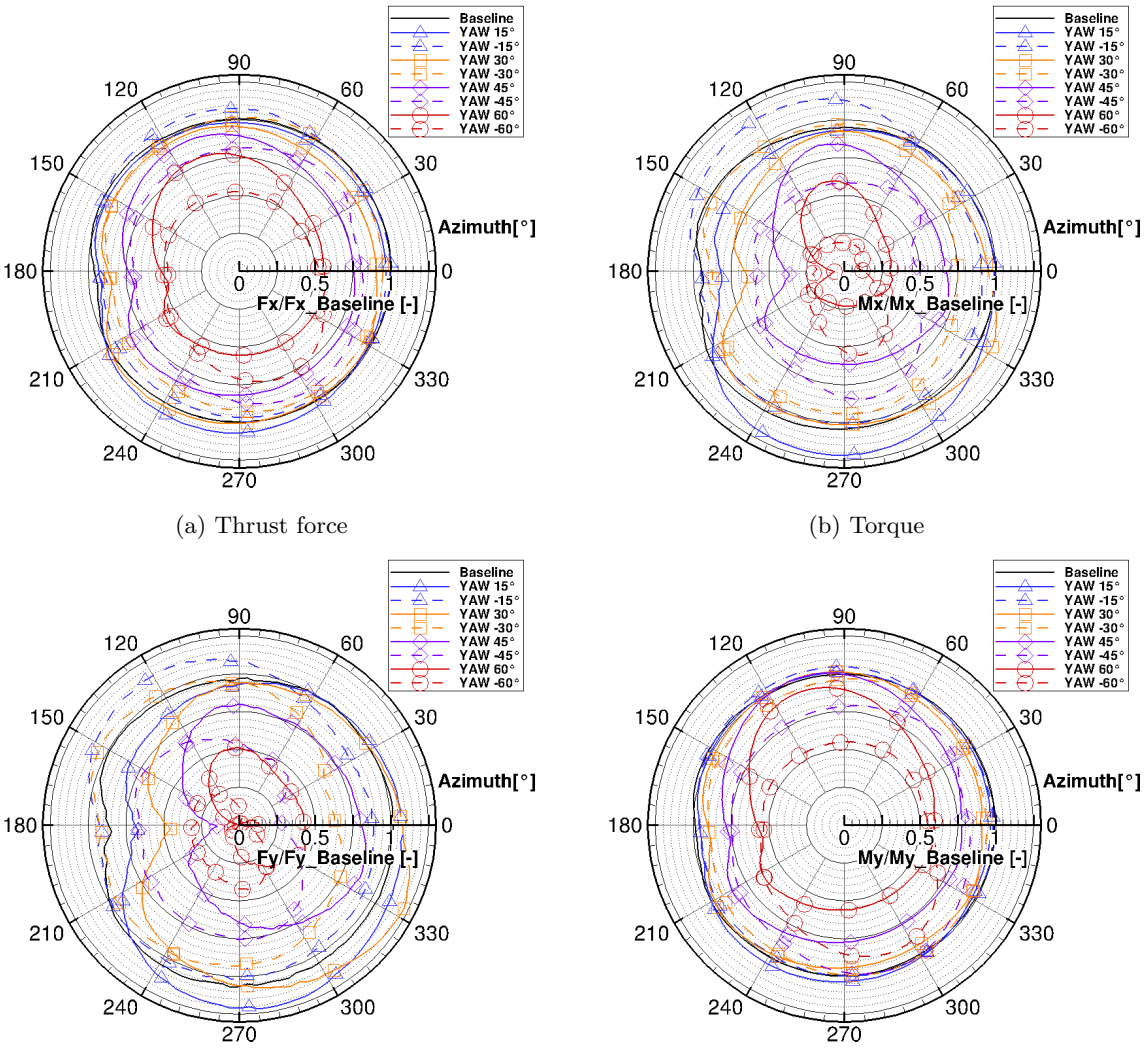

(a) Thrust force

(b) Torque

(c) Edge-wise force

(d) Edge-wise moment

Figure 11: azimuthal variations of the normalized forces and moments of blade 1

3.2.3. Blade loads at a Wind speed of 15 m/sec

Finally, the simulations were performed for a wind speed of 15 m/sec. The blades were pitched with 10.95805° in order to keep the flow attached to the surface of the blade by means of decreasing the angle of attack. The azimuthal variation of the normalized forces and moments are shown in Figure 13. The presented values are normalized by the results of the baseline at the wind speed of 15 m/sec. As shown in Figure 13, for the case of the baseline, the load distributions over one revolution is not symmetric. That is the first difference between this wind speed and the previous ones. The reason for that is the pitch angle in addition to the twist angle which varies from $-14.5°$ to $3.428°$ at the tip. In addition to that is the cone and the tilt angle. All these angles finally affect the angle of attack at the blade sections which might change the load distribution over one revolution for the baseline case. Moreover, for all yaw angles from $+60°$ to $-60°$ the loads are strongly affected by the tower at azimuth angle of $180°$ for blade one. There is decrease of about $15\% - 30\%$ for all loads when blade 1 is crossing the tower. This is because of more decrease in the inflow velocity due to higher wind speed and also because of the blade pitch. Between yaw angles of $+15°$ and $+45°$, there is increase in the load values in the retreating half of the rotor and decrease in the advancing half. Starting from $+45°$, severe tower effect is predicted and the load values becomes negative reaching the minimum value at the azimuth angle of $180°$.

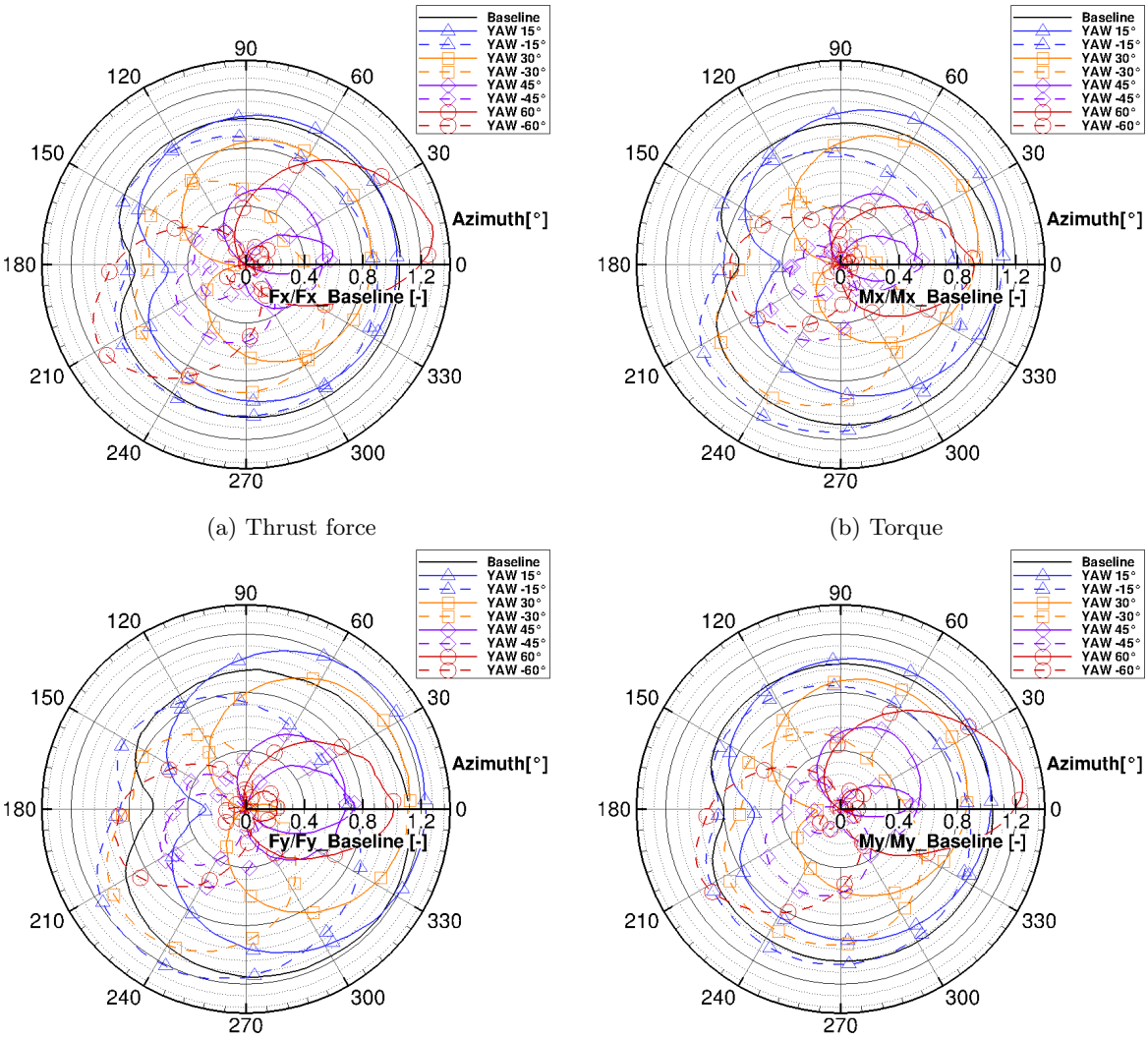

(a) Thrust force

(b) Torque

(c) Edge-wise force

(d) Edge-wise moment

Figure 12: azimuthal variations of the normalized forces and moments of blade 1

These utmost changes in the load values might be critical on the structural vibration of the blades therefore FFT was performed. As shown in Figure 13, all load components have greater amplitude values compared to the previous two cases of low and rated wind speeds. Moreover, for all load components, the amplitude at positive yaw is greater than at negative one. For the normalized flap-wise force and the torque, the largest amplitude is at $\pm 45°$ yaw angle which decreases again at $\pm 60°$. In addition, for the blade twisting moment the largest amplitude is at $\pm 30°$ yaw angle. These ultimate amplitudes will have strong influence on the fatigue and aero-elastic results and should be taken into account.

3.3. Effects of Wind speed on Blade loads

The effect of the wind speed on the distribution of the predicted loads at different yaw angles was investigated. As shown in Figure 14, the below rated wind speeds of 7 m/sec and 11 m/sec have almost the same distribution of the load over one revolution. The presented values are the normalized thrust by the mean value over the blade radius at every wind speed. It is clear that at wind speeds of 7 m/sec and 11 m/sec the distribution is the same for the all positive yaw angles. At 15 m/sec, it is again clear that strong tower influence on the inflow reduction is predicted. The reason for that as discussed before is that the blade is pitched which strongly affect the distribution of the angle of attack over the blade sections.

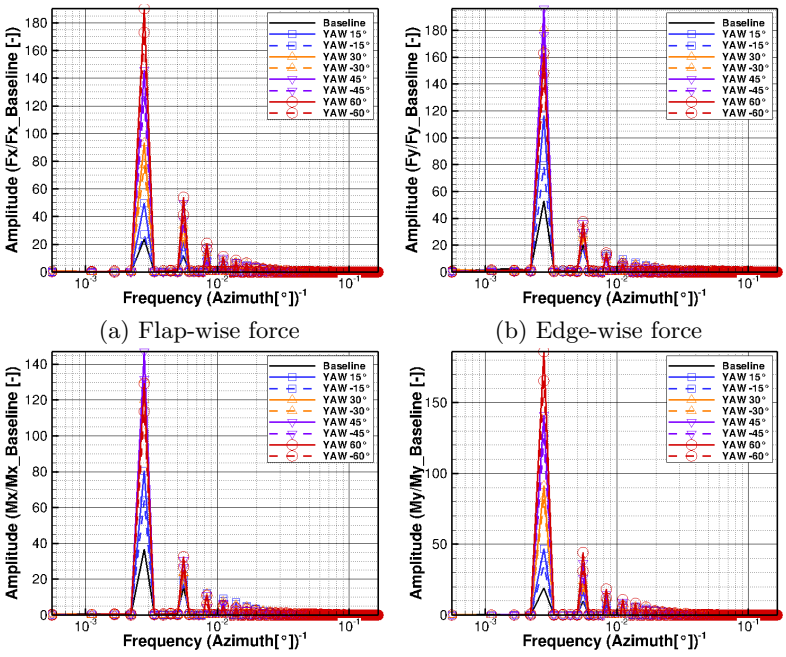

(a) Flap-wise force (b) Edge-wise force

(c) Flap-wise moment (d) Edge-wise moment

Figure 13: FFT of the normalized forces and moments of blade 1

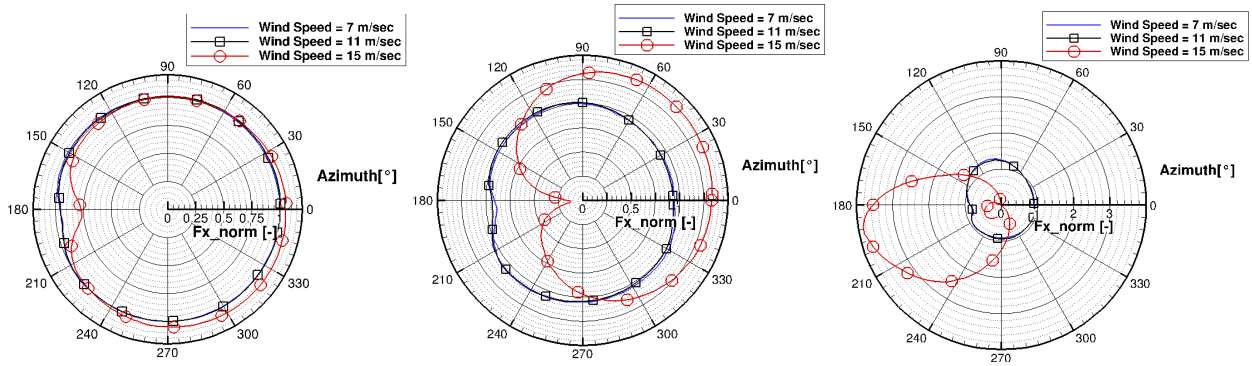

(a) Baseline (b) +30° yaw angle (c) +60° yaw angle

Figure 14: The normalized thrust forces of blade 1 at different wind speeds

4. Conclusion

In this paper, CFD simulations of a yawed large slender bladed HAWT were conducted using a 3D URANS flow solver based on structured overlapped meshes. The Wilcox k-ω turbulence model has been used for the all simulations. Different yawed conditions have been examined ranging from $+60°$ to $-60°$. At the rated wind speed of 11 m/sec and the below rated wind speed of 7 m/sec, time-accurate simulations were conducted. In both cases, as the yaw angle increases to $\pm 15°$, the aerodynamic loads over the blades are slightly increased. This might be because of the stall delay results from the reattachment of the flow over the blade surface. As the yaw angle is further increased above $\pm 15°$, the aerodynamic loads are significantly reduced. The reason for that is that the wind component becomes more aligned tangent to the rotor disk plane. Larger load fluctuations were predicted as the yaw angles were increased.

There is a massive increase in the amplitude at higher yaw angles and the highest amplitudes are in the advancing half on the rotor. These high amplitudes will definitely affect the structural design of the blade and must be taken into account. At wind speeds less than rated wind speed, the yaw angle is the most dominating factor affecting the blade load distributions over one revolution more than the wind speed. It was predicted that the load distributions were the

same with different absolute values. In contrary, at above rated wind speed of 15 m/sec, the wind speed has an utmost effect on the load distributions over one revolution. The reason behind that is the change in the pitch angle which has a great influence on the distribution of the angle of attack along the blade radius.

Acknowledgments
The DAAD (Deutscher Akademischer Austauschdienst) is acknowledged for financial support.

References

[1] Tsalicoglou C, Jafari S, Chokani N and Abhari R 2013 Rans computations of wind turbine near-wake aerodynamics in uniform and yawed inflow *Proceedings of the ASME Turbo Expo* vol 8 (New York, N.Y.: The American Society of Mechanical Engineers) pp 1–12
[2] Duque E P, Burklund M D and Johnson W 2003 *Journal of Solar Energy Engineering* **125** 457–467
[3] Sørensen N N, Michelsen J and Schreck S 2002 *Wind Energy* **5** 151–169
[4] Hansen M O L, Sørensen J N, Voutsinas S, Sørensen N and Madsen H A 2006 *Progress in aerospace sciences* **42** 285–330
[5] Zahle F and Sørensen N N 2007 On the influence of far-wake resolution on wind turbine flow simulations *Journal of Physics: Conference Series* vol 75 (IOP Publishing) p 012042
[6] Sezer-Uzol N and Long L N 2006 *AIAA paper* **394** 2006
[7] Madsen H A, Sørensen N N and Schreck S 2003 Yaw aerodynamics analyzed with three codes in comparison with experiment *ASME 2003 Wind Energy Symposium* (American Society of Mechanical Engineers) pp 94–103
[8] Tongchitpakdee C, Benjanirat S and Sankar L N 2005 *Journal of solar energy engineering* **127** 464–474
[9] Kim D H, Yu D O, Kwon O J, Fletcher T M, Scheurich F and Brown R 2010 Predicting unsteady blade loads of a wind turbine using rans and vorticity transport methodologies *European Wind Energy Conference* pp 33–37
[10] Bak C, Zahle F, Bitsche R, Kim T, Yde A, Henriksen L C, Natarajan A and Hansen M 2013 *DTU Wind Energy Report-I-0092* **5**
[11] Kroll N, Rossow C C, Becker K and Thiele F 2000 *Aerospace Science and Technology* **4** 223–237
[12] Weihing P, Meister K, Schulz C, Lutz T and Krämer E 2014 Cfd simulations on interference effects between offshore wind turbines *Journal of Physics: Conference Series* vol 524 (IOP Publishing) p 012143
[13] Schulz C, Klein L, Weihing P, Lutz T and Krämer E 2014 Cfd studies on wind turbines in complex terrain under atmospheric inflow conditions *Journal of Physics: Conference Series* vol 524 (IOP Publishing) p 012134
[14] Sayed M, Lutz T and Krämer E 2015 Aerodynamic investigation of flow over a multi-megawatt slender bladed horizontal-axis wind turbine *Renewable Energies Offshore* (CRC Press) pp 773–780
[15] Meister K, Lutz T and Krämer E 2009 *EUROMECH [508]-Wind turbine wakes, Madrid*
[16] Wilcox D C 1988 *AIAA journal* **26** 1311–1320
[17] Burton T, Sharpe D, Jenkins N and Bossanyi E 2011 *Wind energy handbook* 2nd ed (John Wiley & Sons) ISBN 9780470699751